Study of regular variations in vertical Total Electron Content (VTEC) from 2013 to 2021 at station BF01 in Ouagadougou

Abstract

This paper presents the regular variations of the Vertical Total Electron Content (VTEC) at station BF01 (Lat. = 12.3714 N and Long. = -1.5197 W) in Ouagadougou (Burkina Faso) located in the trough of the equatorial ionisation anomaly near the northern ridge of the West African zone. The period studied runs from 2013 to 2021. The VTEC is extracted from the raw Global Navigation Satellite System - Continuously Operating Reference Station (GNSS-CORS) data recorded at station BF01 during the study period. The analysis of diurnal variations showed three types of profiles with a dominant profile being the Dome type. Generally speaking, the daily VTEC profiles show a minimum at dawn between 4:00 UT and 6:00 UT followed by a rapid increase from sunrise to a maximum around 15:00 UT, then a gradual decrease in the late afternoon and during the night to reach the minimum just before sunrise. On some days, a second nocturnal maximum is observed between 19:00 UT and 20:00 UT. Seasonal and annual variations revealed that for each year, the highest VTEC values are observed during the equinox, although with higher values at the March equinox. It was also found that the lowest VTEC values are recorded at the summer solstice in each year. The regular variations in the VTEC at station BF01 during the study period therefore highlight three anomalies: the semi-annual anomaly, the equinoctial asymmetry and the winter anomaly. Furthermore, the VTEC at station BF01 in Ouagadougou evolves in phase with the sunspot cycle.

Keywords:*GNSS-CORS; VTEC; Regular variations; Diurnal variations; Seasonal variations; Solar flux F10.7*

1. Introduction

The ionosphere is the ionised part of the Earth's atmosphere that extends from 60 km to 1000 km above the Earth's surface. The main source of ionisation in the ionosphere is the photo-ionisation of the Earth's atmosphere by solar radiation. The ionosphere is a plasma composed of neutral particles (molecules and atoms) and charged particles (electrons and ions). Free electrons in the ionosphere affect the propagation of signals emitted by the Global Navigation Satellite System (GNSS), by altering their speed and direction of travel[47-49]. The ionosphere is a major factor in GNSS positioning and navigation errors, and also affects the telecommunications quality of the waves passing through it. The magnitude of the effect is

proportional to the Total Electron Content (TEC)[1]. The TEC represents the number of free electrons contained in a cylinder with a cross-section of 1 m^2 between the satellite and the ground receiver (Figure 1). It is obtained by integrating the density of free electrons (Ne) in this same cylinder with a height equal to the slant distance between the receiver station R and the transmitting satellite S according to equation (Eq.1) [2].

$$TEC = \int_R^S Ne.dl \qquad \textbf{(Eq.1)}$$

TEC is measured in TECU units, 1 TECU being equal to 10^{16} electrons/m^2.

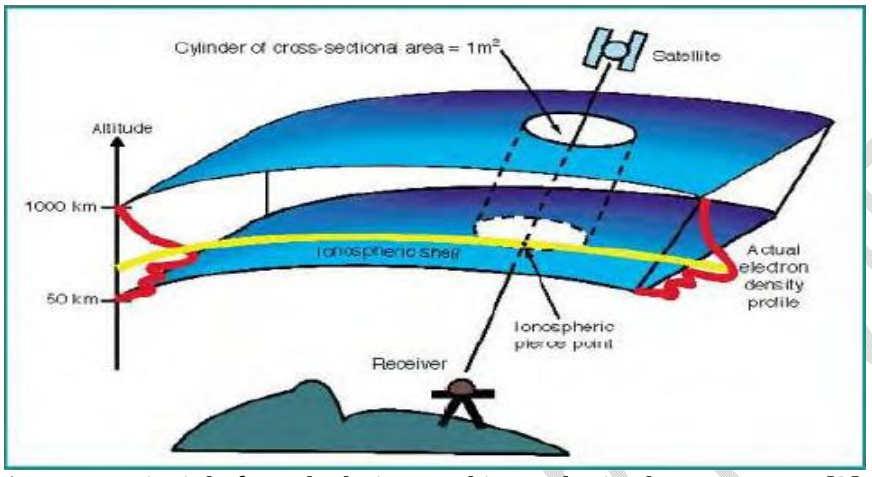

Figure 1: *Principle for calculating total ionospheric electron content*[3].

The RINEX files derived from the GPS data provide the pseudo-distances P_1 and P_2 travelled respectively by the waves with frequencies $f_1 = 1575{,}42\ MHz et f_2 = 1227{,}60\ MHz$ emitted by the satellites to reach the receiver. The Total Slant Electron Content (STEC) is calculated using the relation (Eq.2)[4], [5].

$$STEC = \frac{1}{40{,}3}\left(\frac{f_1^2 . f_2^2}{f_2^2 - f_1^2}\right)(P1 - P2) \qquad \textbf{(Eq.2)}$$

The STEC is then converted to a vertical TEC (VTEC) by considering the ionosphere as a single layer concentrated on a spherical shell of infinitesimal thickness located at an altitude H above the Earth's surface [6], [7], [8], [4]. Figure 2 illustrates this infinitesimal layer approximation at height H above the Earth's surface. The particular geographical position at height H will be noted as IPP, an acronym for 'Ionospheric Pierce Point'. In this work, H is taken equal to 450 km, above the traditional choice of 350km to take into account the plasmasphere. STEC is transformed into VTEC using a translation coefficient (also known as MP for 'Mapping Function') as a function of the angle of elevation β according to the relationship (Eq.3).

$$VTEC = STEC\left(\sqrt{1 - \left(\frac{R_T}{R_T + H}\cos\beta\right)^2}\right)^{-1} \qquad \textbf{(Eq.3)}$$

R_T = 6371,2 km is the average radius of the Earth.

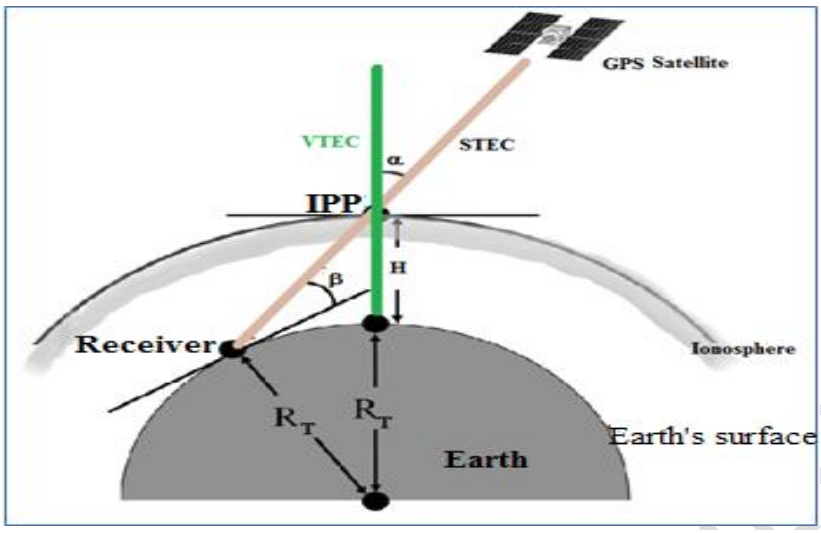

Figure 2: Geometric condition for converting slant TEC into vertical TEC in a thin-film hypothesis for the ionosphere[9]

Ionospheric variations are generally classified into two categories: regular variations and irregular variations [10]. Regular variations occur according to the Earth's rotation and the phases of the solar cycle. These are diurnal, seasonal and annual variations. Irregular variations are mainly the result of solar activity.

Diurnal ionospheric variations are due to the Earth's 24-hour rotation. There is a maximum in the daytime sector, particularly a few hours after local noon. At night, even in the absence of incident solar radiation, a weaker but not zero ionisation, caused by chemical reactions and horizontal and vertical movements, is present[11].

Seasonal ionospheric variations occur due to the tilt of the Earth's rotational axis and the Earth's revolution around the Sun. Over the course of a year, this tilt makes the Earth either leaning towards the Sun, leaning away from the Sun or at an intermediate position between the two. The relative position of the Sun changes from one hemisphere to the other, creating seasons. Three mechanisms are generally invoked to explain the difference in the behaviour of ionospheric parameters in different seasons of the year: the axial mechanism[12], [13], [14], the equinoctial mechanism[15], [16], [13] and the Russell-McPherron mechanism[17].

At low latitudes, the most important ionospheric phenomenon is the equatorial ionisation anomaly (EIA)[18], [19]. The EIA is formed as a result of the diurnal variation of the zonal electric field, which primarily points eastward during the day and reverses at night. With the horizontal northward geomagnetic field at equatorial latitudes, the ionospheric plasma is lifted upward by vertical $\vec{E} \times \vec{B}$ drift [20]. Once the plasma is transported to higher altitudes, it diffuses downward along the geomagnetic field lines into both hemispheres due to gravitational and pressure gradient forces [21], [22] : this is the ‘equatorial fountain’ phenomenon. This

equatorial fountain phenomenon creates the EIA, consisting of a density trough at the equator and two ionisation peaks at latitudes 15° North and 15° South [23].

Numerous studies [24], [25], [26], [18]have been carried out in Africa's equatorial regions to understand ionospheric phenomena and their variability. For most of these studies, the data used come from ionosondes or ionospheric models. Further studies using other types of data are therefore needed to continue the analysis of ionospheric variations in equatorial Africa. In this work, we propose to study regular ionospheric variations using VTEC values. These values are extracted from GNSS-CORS data recorded at station BF01 (Lat. = 12.3714 N and Long. = -1.5197 W) in Ouagadougou over the period 2013 to 2021.The aim of this work is to contribute to a better understanding of the regular ionospheric variations in the equatorial region of West Africa.Details of the station and data, the methodology used and the results obtained are further discussed in the following sections.

2. Data

In this study, the VTEC was determined by using raw satellite data recorded between 2013 and 2021 at the dual-frequency GPS station BF01 (Lat. = 12.3714 N and Long. = -1.5197 W) of Ouagadougou in Burkina Faso. The BF01 GPS station is one of the thirteen permanent stations in the GNSS-CORS network of the Geographic Institute of Burkina Faso (IGB) (https://www.igb.bf/?page_id=47). Figure 3 shows a map of Africa with the geographical positions of station BF01, the magnetic equator and the boundaries of the EIA. Figure 4 shows a map of Burkina Faso with the geographical locations of the 13 receiving stations in the CORS-Burkina network.

The raw data were obtained from the IGB. Measurements taken solely by the GPS system are archived in hourly binary files with a 1s interval. To extract the VTEC, the raw binary satellite data from station BF01, underwent several preliminary processing operations. In a previous publication [27], we explained the process of extracting the VTEC from the raw GNSS-CORS data from the BF01 station.

The geomagnetic activity data used in this document are the daily geomagnetic indices aa downloaded from https://isgi.unistra.fr/indices_aa.php.These aa indices were used to determine the most magnetically quiet days.

We used the annual average of the new version of the sunspot number (SN) to determine the different phases of the solar cycle. The daily solar radio flux at 2800 MHz from Ottawa (F10.7) is used to study the variation of the VTEC as a function of solar activity. The solar index SN and F10.7 data are downloaded from the NASA OMNIWeb website: https://omniweb.gsfc.nasa.gov/form/dx1.html.

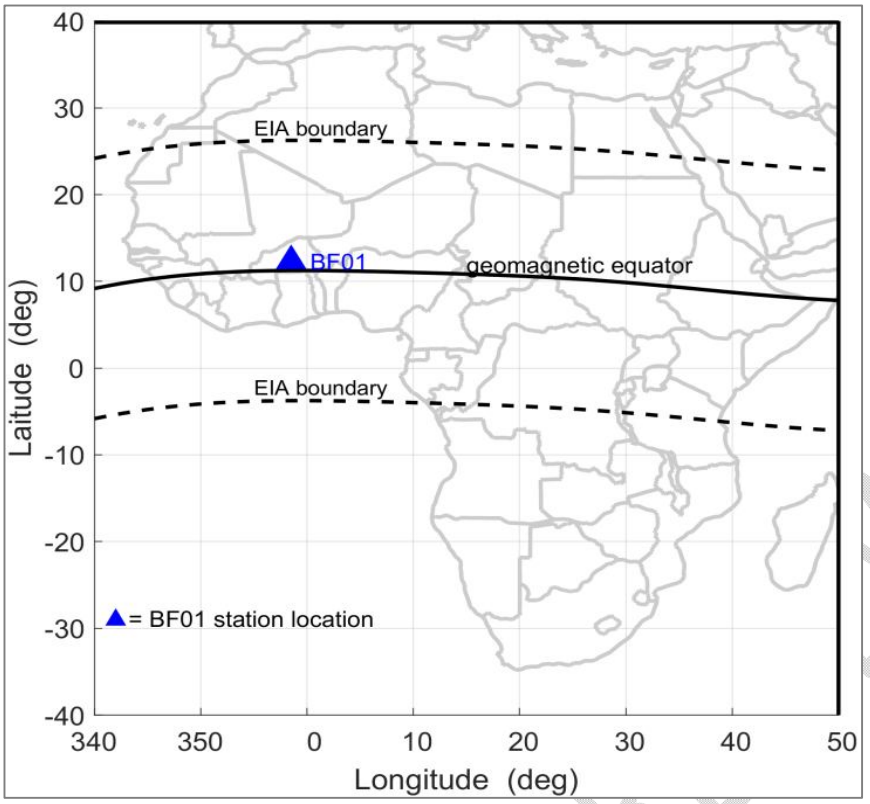

Figure 3: *Map of Africa with location of BF01 station*

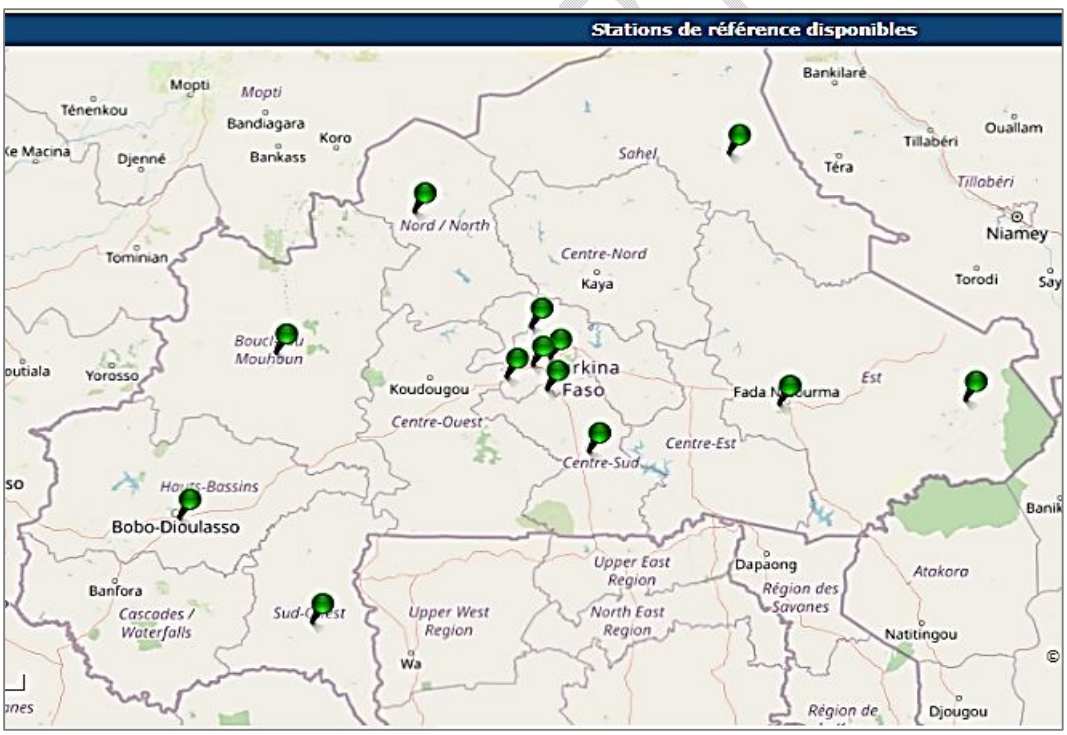

Figure 4: *Map of the network of 13 GNSS-CORS receiving stations in Burkina Faso (www.bfcors.net)*

3. Methodology

Our methodology indicates the process used to process the VTEC and to determine the seasons, the quietest day of the year and the different phases of a solar cycle.

3.1 VTEC processing

The measurements are recorded in universal time (UT). To highlight and analyse regular ionospheric variations, we first calculated the monthly and seasonal median VTEC values and produced graphs showing the monthly and seasonal VTEC profiles. Secondly, we produced simple 2D graphical representations of daily VTEC values to observe daily variations. Finally, a third type of figure is obtained by plotting the average monthly VTEC values from 2013 to 2021 and superimposing the variation in the F10.7 cm solar flux index. This graph shows how the monthly VTEC varies from year to year, and also how the monthly median VTEC changes with solar activity.

3.2. Determination of seasons

In order to study seasonal variations in VTEC, each year was divided into seasons. Following the methods of [18], [28], [29], the seasons considered are the March-April equinox, the September-October equinox, the summer solstice (May, June, July and August) and the winter solstice (November, December, January and February). .

3.3. Determination of solar cycle phases

The phases of the solar cycle were determined by applying the criteria defined by[30] on the values of the annual averages of the new version of the sunspot number (SN) data. According to these authors, a solar cycle is subdivided into four phases defined as follows:

- minimum phase: $SN(t) < 0{,}122.SN_{max}$;
- ascending phase: $0{,}122.SN_{max} \leq SN(t) \leq 0{,}73.SN_{max}$;
- maximum phase: $SN(t) > 0{,}73.SN_{max}$and
- descending phase: $0{,}73.SN_{max} \geq SN(t) > SN_{min(nextcycle)}$.

$SN(t), SN_{max} et SN_{min}$are respectively the annual mean value of sunspot numbers in a given year, the maximum value of sunspot numbers in a given solar cycle and the minimum value of sunspot numbers in the next solar cycle. Table 1 gives an overview of the solar cycles and phases for the period 2013 - 2021.

Table 1:*Distribution of years by solar phase*

Cycles	**Cycle 24**				**Cycle 25**
Phases	Ascending	Maximum	Descending	Minimum	Minimum

Années	2013	2014	2015-2016-2017	2018-2019	2020-2021

3.4. Determination of quiet days

Quiet days were determined on the basis of the criterion for determining days of geomagnetic activity developed by [31]. According to this criterion, days of calm activity correspond to days on which the daily mean values of the aa index (Aa) are such that Aa < 20 nT. The other days corresponding to Aa ≥ 20 nT are days of disturbed activity. We first determined the quietest day of each month (day with the lowest value of Aa). If the lowest values of Aa are equal on several days, we look for the average of aa over 48 hours before and after each of these days. The quietest day is one where the average values of aa over 48 hours before and after that day are the lowest.So we have 12 quiet days for each year. We then looked for the quietest day among the 12 quiet days selected for each year by applying the same criterion. For the period 2013 to 2021, we have therefore selected 9 quiet days. Table 2 summarises the 9 quiet days selected over the study period. The table also contains the highest and lowest VTEC values and the times at which these values are recorded for each day.

Table 2:*Quietest days of each year with the highest and lowest VTEC values and their corresponding times*

Date		05/10/13	19/01/14	20/06/15	21/10/16	14/02/17	21/05/18	19/04/19	30/04/20	05/05/21
VTEC	tecu	53,06	49,58	42,39	33,44	28,65	20,60	25,96	25,92	26,90
Max	Time	15 :52	13 :52	14 :52	15 :07	15 :22	14 :52	12 :37	16 :37	13 :04
VTEC	tecu	9,57	3,95	6,15	3,18	3,86	3,37	4,69	4,07	4,20
Min	Time	04 :52	05 :37	04 :52	05 :22	4 :22	4 :22	5 :22	3 :37	4 :37

4. Results and discussion

4.1. Variation of VTEC with the solar cycle

Figure 5 shows the variation in average monthly VTEC values (in grey) for all the months of each year from 2013 to 2021, with the variation in the F10.7 cm solar flux index (in red) superimposed and scaled on the right.

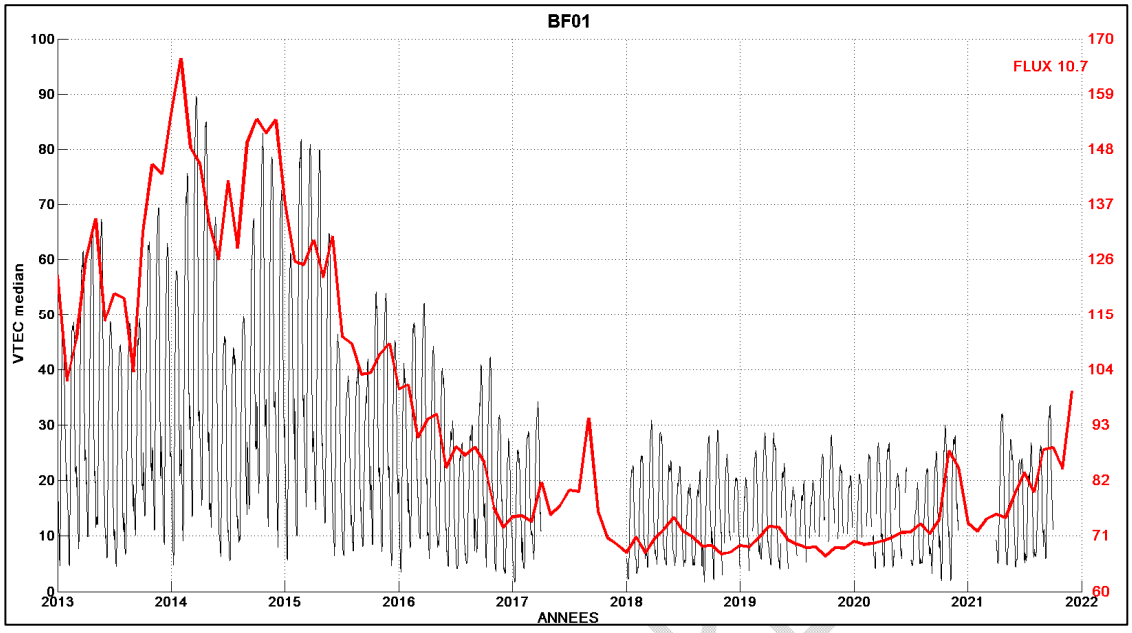

Figure 5: *Variation in the monthly VTEC at station BF01 and solar flux F10.7 from 2013 to 2021*

We observe in Figure 5 a general increasing trend in VTEC from 2013 to 2014 with a maximum peak of 90 TECU reached in 2014. During the same period, F10.7 flux values increase and reach a maximum of 165 sfu in 2014. Between 2014 and 2019, the maximum monthly VTEC values decrease fairly rapidly, reaching a minimum of 20 TECU at the end of 2019. This general downward trend can also be seen in the variation in the F10.7 solar index over the period 2015-2017, which corresponds to the downward phase of cycle 24 (see Table 1). The figure clearly shows that the low values of the VTEC and the F10.7 flux are observed between 2018 and 2020. From 2020 onwards, VTEC max and F10.7 values rise slightly together again.

In general, over the period studied, variations in VTEC and F10.7 solar flux follow the same trend. We can clearly see the peak in VTEC in the years 2014/2015 and the minima in VTEC in the years 2018-2019, corresponding respectively to the maximum and minimum of solar cycle 24. The maximum monthly VTEC values calculated at station BF01 therefore vary according to the phases of the solar cycle, with an ascending phase, a descending phase, a maximum and a minimum.

This variability in the VTEC according to the solar cycle is more or less predictable because the intensity of solar UV radiation varies according to solar activity[28]. It is highest at solar maximum and lowest at solar minimum. This UV solar radiation causes photo-ionisation, which produces electrons and consequently increases the electron density, and hence the VTEC. Our results are in line with previous work.[32] and[33] studied the variation of the TEC at the level of the African equatorial anomaly region during the period from 2009 to 2016 of solar cycle 24. They show that the TEC increases each year from solar minimum to solar

maximum. More recently,[34] report that the TEC increases progressively from the solar minimum (Nov. 2008-2010) and throughout the ascending solar phase (2011-2013) until the solar maximum (2014-2015) when it reaches its maximum and gradually decreases from 2015-2016 corresponding to the descending phase of solar cycle 24.

4.2. Annual and seasonal variations in VTEC

Figure 6 shows a 2D graph of daily variations in VTEC for each year. The VTEC is represented by a colour, the scale of which is shown on the right of the figure. The x-axis is the day, with only the first day of the month indicated by the month number, and the y-axis is the UT time. Unfilled areas (white background) reflect missing data for these periods. This representation makes it possible to visualise diurnal and seasonal variations in VTEC and to follow its evolution from one year to the other.

The graphs in Figure 7 show the temporal variations in average seasonal VTEC values for the four seasons for each year of the period studied (2013 to 2021). This figure shows a variation in the amplitude of the seasonal average VTEC values from one year to the next. Figure 6 provides a good overview of the changes in VTEC over the different seasonal periods. It clearly shows that in all years, night-time values are lower than daytime values, with peaks between 12:00 UT and 16:00 UT. We note that there is a difference in the behavior of VTEC depending on the years and seasons. The year 2014 (maximum in cycle 24) records the highest VTEC values (sometimes reaching 100 TECU). Figure 7 also shows a difference between the VTEC values of the different seasons during the period studied. In general, Figures 6 and 7 show that over the entire study period, the VTEC values of the equinoxes are higher than those of the solstices, and the lowest values are observed during the summer solstices. The March equinoxes record higher VTEC values than the autumn equinoxes. VTEC values therefore vary from one equinox to the next and from one solstice to the other. The figures therefore reveal three types of anomalies in the seasonal variation in VTEC at station BF01 during the study period:(1) the semi-annual anomaly, where VTEC values are higher at the equinoxes than at the solstices[35]. (2) the equinoctial asymmetry, where the VTEC peaks are different from one equinox to the next[36]. In our case, the peaks at the March equinox are higher than those at the September equinox. (3) the last is the winter or ‘seasonal’ anomaly, where the VTEC values in winter are higher than those in summer [37].The various anomalies observed were much more pronounced in 2014 than in other years. This could be explained by the fact that 2014 is a year of maximum solar activity in a solar cycle. Between 2016 and 2021 (period of lowest solar activity), the various anomalies seem to decrease in intensity or even disappear. The evolution of the amplitude of the various anomalies would therefore depend on the solar activity cycle.

Similar results were obtained by other previous studies[38], [28], [39], [40], which have invoked the axial mechanism, the equinoctial mechanism and the Russell-McPherron mechanism to explain the various anomalies observed.[18] and [39]attributed the existence of the equinoctial asymmetry between the March and September equinoxes to the variation in solar wind speeds, atmospheric temperature, thermospheric composition and density, and the oxygen-nitrogen (O/N_2) ratio in the atmosphere from one equinox to the other. Their study showed that the O/N_2 ratio and the neutral temperature are greater at one equinox than at the other. This could also explain the existence of the equinoctial asymmetry observed in the present study. For[42], the O/N_2 ratio increases during the equinoxes leading to a greater electron density and, consequently, ionisation should be more developed during the equinoxes than during the solstices. This could be at the origin of the semi-annual anomaly observed at station BF01. This anomaly could be explained by the fact that during the equinoctial months, the sun is above the equator and the temperature at the equator is higher than at the pole.

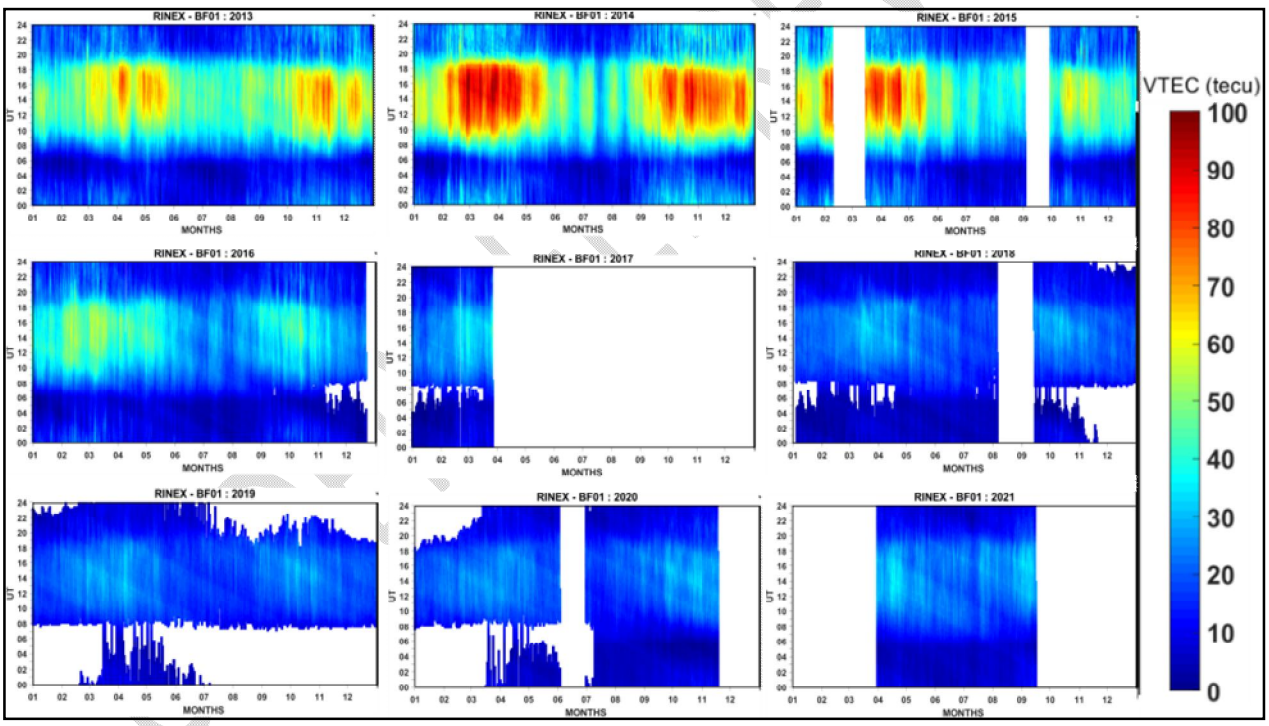

Figure 6 : Seasonal VTEC evolution in 2D at station BF01 for the years 2013 to 2021

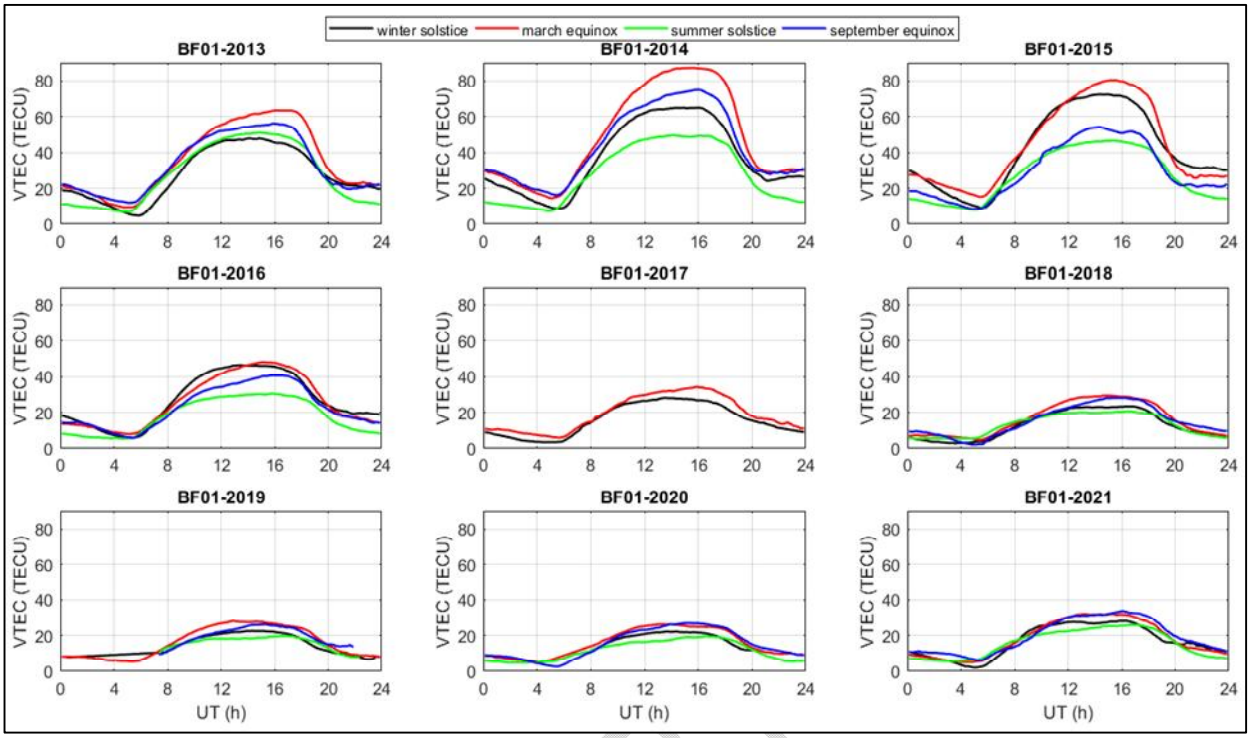

Figure 7 :*Seasonal variation in VTEC according to the time of day (UT) at station BF01 for the years 2013 to 2021*

4.3. Diurnal variation in VTEC

Figure 8 shows the daily variations in VTEC over one month (January 2013) taken as a test over the study period. This figure showsthe daily diurnal variation over a month and allows visual observation of all the daily VTEC profiles. A 24-hour cyclical variation can be seen, corresponding to the Earth's rotation. The night-time minima are all below 10 TECU. The

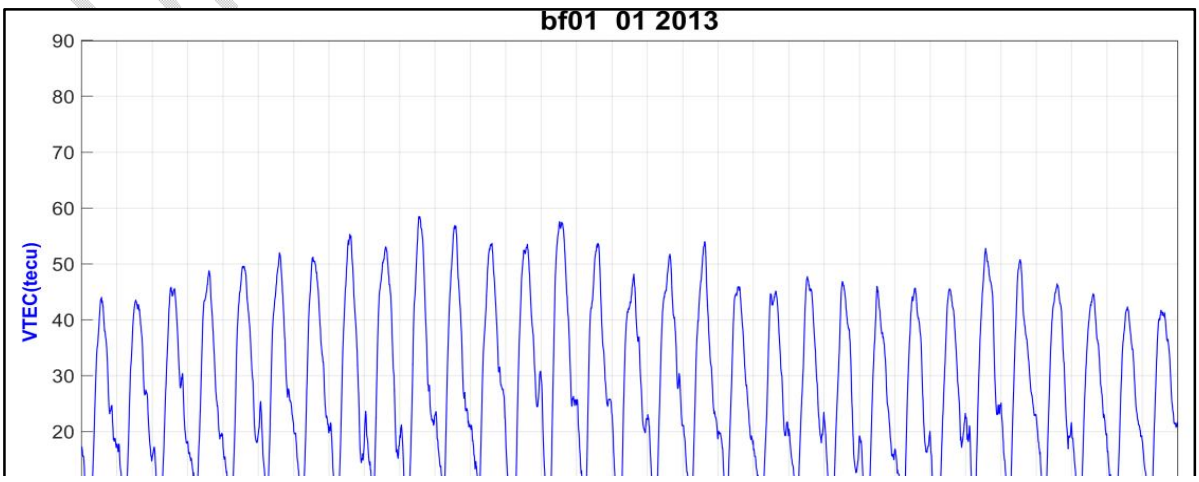

maxima show a sinusoid with a maximum around 10-14 January and the lowest values at the end of the month. This period of 27/30 days could be linked to the Sun's rotation period.

To better see and identify the daily variability of VTEC, we have retained the magnetically quietest day during each year (see paragraph 3.4). The daily variation of each of the 9 quiet days selected is then plotted in Figure 9. This figure clearly showsthe evolution of VTEC hour by hour for each day and permits to draw a general trend.

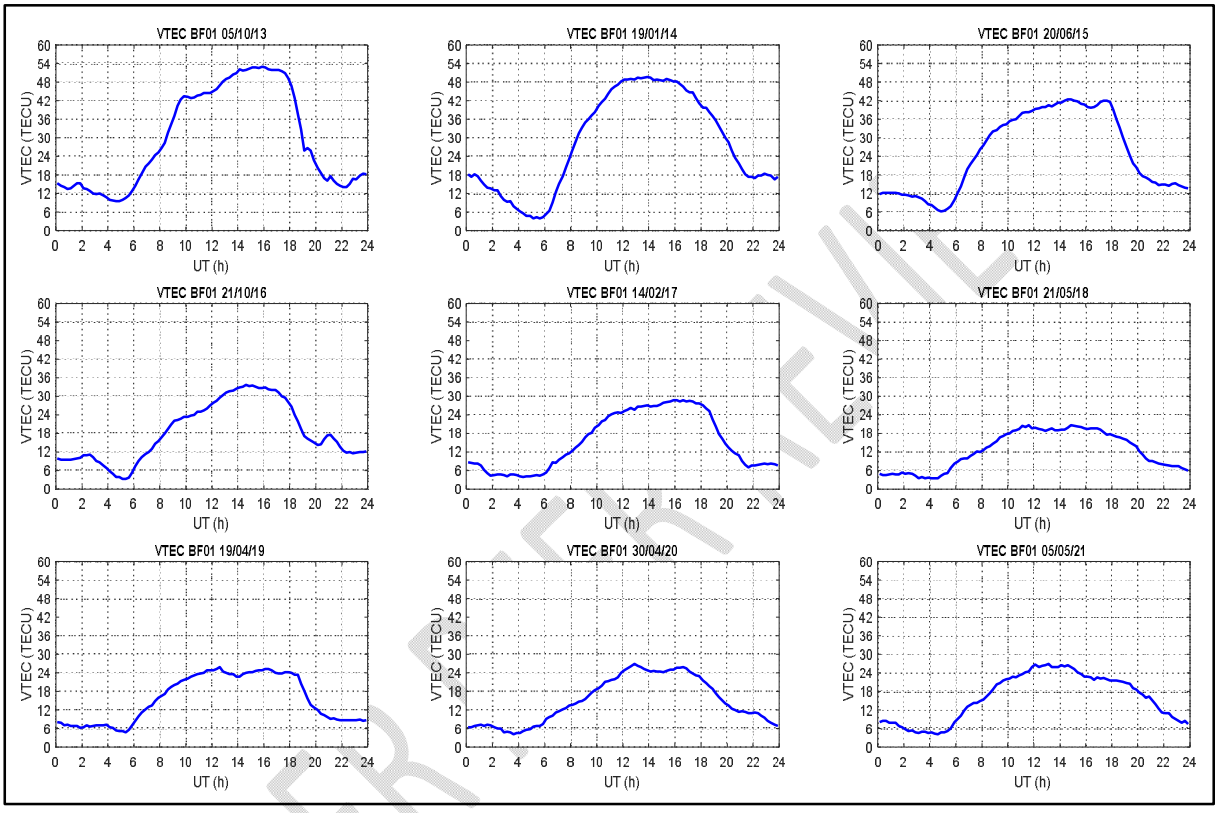

Figure 9 : Daily variation in VTEC as a function of TU at station BF01 for 9 selected quiet days in the period 2013 to 2021

All the profiles show that the VTEC has a minimum around 5:00 UT and increases rapidly from 06:00 UT to reach a maximum around 15:00 UT. Between 16:00 UT and 20:00 UT, the VTEC decreases rapidly. This decrease continues, but slowly, between 20:00 UT and 06:00 UT (during the night) to reach a minimum around 05:00 UT, before sunrise.However, the minimum and maximum values occur at different times, as shown in Table 2.The VTEC daily variation profiles are essentially of three types: bell-shaped curves representing a single peak (dome-type profile), plateau-shaped curves and curves with two maximum peaks. Dome curves are the most dominant. According to [43], [44], who described the physics of the different shapes of the EIA VTEC curves in the African sector, and according to [45], these different shapes of curves reflect the presence or absence of electric currents in the equatorial ionosphere (equatorial electrojet and equatorial counter-electrojet), with reference to the daily variation in

electric current under calm weather conditions. Dome-type profiles characterise an absence of equatorial electrojet (e.g. on 19/01/20214), while the 'plateau' profile reveals the presence of a weak electrojet (e.g. on 14/02/2017) and the profile with the two peaks reflects the presence of a strong electrojet (e.g. on 30/04/2020).[46] and[29] who conducted studies on the diurnal behaviour of NmF2, using the databases of several solar cycles respectively in Ouagadougou/Burkina Faso and Phu Thuy/Vietnam on the northern ridge of the equatorial fountain in Vietnam have shown that near the magnetic equator we find the shape of the two peaks, and at the ridge we find the bell shape. The geographical location of station BF01 (in the trough of the EIA and near the northern peak) could explain our results: the presence of curve shapes with a predominance of the bell shape.

On certain days (e.g. 05/10/13; 21/10/2016 in Figure 9), the diurnal evolution of the VTEC at station BF01 shows a peculiarity with a slight rise in the VTEC after 20:00 UT, leading to a slight peak around 21:00 UT. This peak after sunset is generated by the Pre-Reversal Enhancement (PRE), which creates a strong vertical drift in $\vec{E}\mathrm{x}\vec{B}$. Previous work[38], [28] done in the equatorial region also observed this peak after sunset and concluded that PRE generates a brief increase in electron density at the F2 layer just after sunset between 18:00 UT and 21:00 UT.

In general, the VTEC values reach a minimum before dawn, increasing steadily from sunrise to reach a maximum around 15:00 UT. They then decrease progressively after sunset to reach a minimum just before sunrise. Our results are in agreement with previous work in the African equatorial region by authors such as[32], [38], [18] who estimated that these diurnal variations in the VTEC are characteristic of the low-latitude ionosphere during quiet periods. The addition of the VTEC morphology at station BF01 confirms the previous results.

This observed diurnal profile of the VTEC confirms the continuity equation[47] which governs the formation of the ionosphere. At sunrise, the production term, i.e. the creation of free electrons under the action of EUV, UV and X-ray radiation, is immediate and rapid. As the VTEC is directly linked to the density of electrons in the ionospheric plasma, it begins to increase, reaching its maximum in the afternoon. After sunset, the production term disappears and the loss rate becomes dominant.[32] have also suggested that diurnal VTEC behaviour is caused by changes in the magnetic field tube. The total magnetic field tube is very small at equatorial and low latitudes, the electron content of the field tubes decreases rapidly after sunset in response to the low temperature of the thermosphere during the night. After sunrise, the magnetic field tubes fill up again rapidly because of their small volume, leading to a sharp increase in ionisation. This could explain the diurnal behaviour of the VTEC observed at station BF01.

5. Conclusion

This study focuses on the regular variations from 2013 to 2021 of the VTEC extracted from GNSS-CORS data from station BF01 (Lat. = 12.3714 N and Long. = -1.5197 W) in Ouagadougou, Burkina Faso. The results show that the morphologies of the daily variation of the VTEC studied are of three types (bell-shaped curves (dome), plateau-shaped curves and curves with two maximum peaks) with a predominance of dome-shaped profiles. The VTEC was found to have a minimum around 05:00 UT and to increase rapidly from 06:00 UT to reach a maximum around 15:00 UT. Between 16:00 UT and 20:00 UT, there is a real decrease in the VTEC. This decrease continues but more slowly between 20:00 UT and 06:00 UT to reach a minimum around 05:00 UT, before sunrise. Diurnal maxima vary from one day to the other, and also according to the season and the different years. The present study also revealed on some days the presence of a second VTEC peak after 20:00 UT, which is an indicator of the 'Pre-Reversal Enhancement' phenomenon. The annual and seasonal studies revealed three types of anomalies: the seasonal anomaly; the equinoctial asymmetry and the winter anomaly. The highest values are observed at the March equinoxes and the lowest values at the summer solstices. It has also been shown that variations in the VTEC at station BF01 occur according to the solar activity and follow the same phases as the solar cycle.

Disclaimer (Artificial intelligence)

Option 1:

Author(s) hereby declare that NO generative AI technologies such as Large Language Models (ChatGPT, COPILOT, etc) and text-to-image generators have been used during writing or editing of manuscripts.

Option 2:

Author(s) hereby declare that generative AI technologies such as Large Language Models, etc have been used during writing or editing of manuscripts. This explanation will include the name, version, model, and source of the generative AI technology and as well as all input prompts provided to the generative AI technology

Details of the AI usage are given below:

1.

2.

3.

References

[1] M. S. Bagiya, H. P. Joshi, K. N. Iyer, M. Aggarwal, S. Ravindran, et B. M. Pathan, « TEC variations during low solar activity period (2005–2007) near the Equatorial Ionospheric Anomaly Crest region in India », *Ann. Geophys.*, vol. 27, n° 3, p. 1047‑1057, mars 2009, doi: 10.5194/angeo-27-1047-2009.

[2] J. A. Klobuchar, Total electron content studies of the ionosphere, vol. 73, n° 98. Air Force Cambridge Research Laboratories, Air Force Systems Command, United …, 1973.

[3] A. Tachema, « Modélisation en 3D de la couche ionosphérique par des données GPS: utilisation d'estimateurs des moindres carrés et du filtre de Kalman », *Mém. Magister En Géod. Cent. Tech. Spatiales Oran Algér.*, 2012.

[4] R. Fleury, « GPS / IONOSPHERE. Working Session 2: Traitement Mesures GPS Rinex & Fichiers DCB », in *Communication*, Rabat - Maroc, 2017.

[5] N. Ya'acob, M. Abdullah, M. Ismail, M. Ibrahim, et Z. Zakaria, « Total Electron Content (TEC) and Estimation of Positioning Error Using Malaysia Data », *Proc. World Congr. Eng. 2010*, vol. Vol I, n° WCE 2010, June 30-July 2, 2010.

[6] J. Fraile-Ordonez, « Real-time TEC determination for ionospheric modeling in WADGPS », in *Proceedings of the 8th International Technical Meeting of the Satellite Division of The Institute of Navigation (ION GPS 1995)*, 1995, p. 1193‑1197.

[7] N. Jakowski, « Generation of TEC maps over the COST 251 area based on GPS measurements », 1998.

[8] S. Schaer, *Mapping and predicting the Earth's ionosphere using the Global Positioning System*, Société helvétique des sciences naturelles. Commission géodésique 130.92.252.184. in Société helvétique des sciences naturelles, 1999.

[9] W. Z. Hein, Y. Goto, et Y. Kasahara, « Estimation Method of Ionospheric TEC Distribution using Single Frequency Measurements of GPS Signals », *Int. J. Adv. Comput. Sci. Appl.*, vol. 7, n° 12, 2016.

[10] M. Rajabi, A. Amiri-Simkooei, H. Nahavandchi, et V. Nafisi, « Modeling and prediction of regular ionospheric variations and deterministic anomalies », *Remote Sens.*, vol. 12, n° 6, p. 936, 2020, doi: doi:10.3390/rs12060936.

[11] A. Leick, L. Rapoport, et D. Tatarnikov, *GPS satellite surveying*. JOHN WILEY & SONS, INC, 2015.

[12] N. A. Barkhatov, A. E. Levitin, E. A. Revunova, et A. B. Vinogradov, « Geomagnetic activity of magnetic clouds considering season of year », *Phys. Auror. Phenom. Proc XXXVII Annu. Semin. Apatity Pp 78-80 2014*, 2014.

[13] E. W. Cliver, L. Svalgaard, et A. G. Ling, « Origins of the semiannual variation of geomagnetic activity in 1954 and 1996 », *Ann. Geophys.*, vol. 22, n° 1, p. 93‑100, janv. 2004, doi: 10.5194/angeo-22-93-2004.

[14] A. Cortie, « Sun-spots and terrestrial magnetic phenomena, 1898-1911 », *Mon. Not. R. Astron. Soc. Vol 73 P 52*, vol. 73, p. 52, 1912.

[15] J. Bartels, « Terrestrial-magnetic activity and its relations to solar phenomena », *Terr. Magn. Atmospheric Electr.*, vol. 37, n° 1, p. 1‑52, 1932.

[16] L. Svalgaard, « Geomagnetic activity: Dependence on solar wind parameters », Rapport, 1977.

[17] C. Russell et Rl. McPherron, « Semiannual variation of geomagnetic activity », *J. Geophys. Res.*, vol. 78, n° 1, p. 92‑108, 1973.

[18] B. Oryema, E. Jurua, F. M. D'ujanga, et N. Ssebiyonga, « Investigation of TEC variations over the magnetic equatorial and equatorial anomaly regions of the African sector », *Adv. Space Res.*, vol. 56, n° 9, p. 1939‑1950, nov. 2015, doi: 10.1016/j.asr.2015.05.037.

[19] A. O. Hammou, S. Makhlouf, H. Abdellaoui, et N. Zaourar, « Characteristics of the ionospheric total electron content of the equatorial ionization anomaly in the three sector longitude », *Bull. Sci. Géographiques INCT*, vol. 27, n° 1, p. 48‑51, 2023.

[20] E. N. Bramley et M. Peart, « Diffusion and electromagnetic drift in the equatorial F 2 region », *J. Geophys. Res.*, vol. 69, n° 21, p. 4609‑4616, 1964.

[21] M. C. Kelley, *The Earth's ionosphere: Plasma physics and electrodynamics*. Academic press, 2009.

[22] X. Wang, J.-J. Berthelier, et J. P. Lebreton, « Ionosphere variations at 700 km altitude observed by the DEMETER satellite during the 29 March 2006 solar eclipse », *J. Geophys. Res. Space Phys.*, vol. 115, n° A11, 2010.

[23] E. V. Appleton, « Two anomalies in the ionosphere », *Nature*, vol. 157, n° 3995, p. 691‑691, 1946.

[24] F. Ouattara et R. Fleury, « Variability of CODG TEC and IRI 2001 total electron content (TEC) during IHY campaign period (21 March to 16 April 2008) at Niamey under different geomagnetic activity conditions », *Sci. Res. Essays*, vol. 6, n° 17, p. 3609‑3622, 2011.

[25] A. Adewale, E. Oyeyemi, P. Cilliers, L. McKinnell, et A. Adeloye, « Low solar activity variability and IRI 2007 predictability of equatorial Africa GPS TEC », *Adv. Space Res.*, vol. 49, n° 2, p. 316‑326, 2012.

[26] C. Zoundi, F. M. Ouattara, R. Fleury, C. Amory-Mazaudier, et P. Lassudrie-Duchesne, « Seasonal TEC variability in West Africa equatorial anomaly region », *Eur. J. Sci. Res.*, vol. 77, n° 3, p. 309‑319, 2012.

[27] P. Ouédraogo, G. Karim, D. Abidina, F. Rolland, et O. Frédéric, « Extraction of ionospheric vertical total electron content (VTEC) using global navigation satellite system-continuously operating reference station (GNSS-CORS) data from station BF01 in Ouagadougou », *Int. J. Phys. Sci.*, vol. 19, n° 1, p. 26‑34, mars 2024, doi: 10.5897/IJPS2023.5065.

[28] I. Azzouzi, « Impact des évènements solaires sur l'ionisation de l'ionosphère des moyennes et basses latitudes dans le secteur Europe-Afrique », Université Pierre et Marie Curie-Paris VI; Université Mohammed V (Rabat), 2016.

[29] H. Pham Thi Thu, C. Amory-Mazaudier, et M. Le Huy, « Time variations of the ionosphere at the northern tropical crest of ionization at Phu Thuy, Vietnam », n° 1, p. 197‑207, 2011.

[30] S. Sawadogo, D. A. Gnabahou, T. Pahima, et F. Ouattara, « Solar activity: Towards a standard classification of solar phases from cycle 1 to cycle 24 », *Adv. Space Res.*, vol. 73, n° 1, p. 1041‑1049, janv. 2024, doi: 10.1016/j.asr.2023.11.011.

[31] F. Ouattara et C. Amory-Mazaudier, « Solar–geomagnetic activity and Aa indices toward a standard classification », *J. Atmospheric Sol.-Terr. Phys.*, vol. 71, n° 17‑18, p. 1736‑1748, 2009.

[32] V. Chauhan, O. P. Singh, et B. Singh, « Diurnal and seasonal variation of GPS-TEC during a low solar activity period as observed at a low latitude station Agra », *9420 Dv 9660 Qd*, 2011.

[33] S. Oron, F. M. D'ujanga, et T. J. Ssenyonga, « Ionospheric TEC variations during the ascending solar activity phase at an equatorial station, Uganda », *Indian J. Radio Space Phys.*, vol. Vol 42, févr. 2013.

[34] T. S. Oluwadare, C. Nguyen Thai, A. O.-O. Akala, S. Heise, M. Alizadeh, et H. Schuh, « Characterization of GPS-TEC over African equatorial ionization anomaly (EIA) region during 2009–2016 », *Adv. Space Res.*, vol. 63, n° 1, p. 282‑301, janv. 2019, doi: 10.1016/j.asr.2018.08.044.

[35] J. Titheridge, « The electron content of the southern mid-latitude ionosphere, 1965–1971 », *J. Atmospheric Terr. Phys.*, vol. 35, n° 5, p. 981‑1001, 1973.

[36] N. Balan, Y. Otsuka, G. J. Bailey, et S. Fukao, « Equinoctial asymmetries in the ionosphere and thermosphere observed by the MU radar », *J. Geophys. Res. Space Phys.*, vol. 103, n° A5, p. 9481‑9495, mai 1998, doi: 10.1029/97JA03137.

[37] H. Rishbeth et C. Setty, « The F-layer at sunrise », *J. Atmospheric Terr. Phys.*, vol. 20, n° 4, p. 263‑276, 1961.

[38] O. S. Bolaji, J. O. Adeniyi, S. M. Radicella, et P. H. Doherty, « Variability of total electron content over an equatorial West African station during low solar activity: variation of tec over an equator », *Radio Sci.*, vol. 47, n° 1, p. n/a-n/a, févr. 2012, doi: 10.1029/2011RS004812.

[39] F. Ouattara, J. L. Zerbo, M. Kaboré, et R. Fleury, « Investigation on equinoctial asymmetry observed in Niamey Station Center for Orbit Determination in Europe Total Electron Content (CODG TEC) variation during ~ solar cycle 23 », *Int. J. Phys. Sci.*, vol. 12, n° 22, p. 308‑321, nov. 2017, doi: 10.5897/IJPS2017.4684.

[40] K. Guibula, F. Ouattara, et D. A. Gnabahou, « foF2 seasonal asymmetry time variation at Korhogo station from 1992 to 2002 », *Int. J. Geosci.*, vol. 9, n° 04, p. 207, 2018.

[41] A. Kherani, O. Jonah, et E. de Paula, « Observations and simulations of equinoctial asymmetry during low and high solar activities », in *13th International Congress of the Brazilian Geophysical Society & EXPOGEF, Rio de Janeiro, Brazil, 26–29 August 2013*, Society of Exploration Geophysicists and Brazilian Geophysical Society, 2013, p. 1906‑1909.

[42] J. Vassal, « Electrojet, contre-électrojet et région F à Sarh (Tchad) », *Géophysique ORSTOM Paris*, 1982a.

[43] J. Vassal, « La variation du champ magnétique et ses relations avec l'électrojet équatorial au Sénégal Oriental », in *Annales Geophysicae*, 1982b, p. 347‑355.

[44] J. Faynot et P. Vila, « F region strata at the Magnetic Equator », *Ann. Geophys.*, p. 1‑9, 1979.

[45] F. Ouattara et C. Amory-Mazaudier, « Statistical study of the equatorial F2 layer critical frequency at Ouagadougou during solar cycles 20, 21 and 22, using Legrand and Simon's classification of geomagnetic activity », *J. Space Weather Space Clim.*, vol. 2, p. A19, 2012.

[46] S. Chapman, « The absorption and dissociative or ionizing effect of monochromatic radiation in an atmosphere on a rotating earth », *Proc. Phys. Soc.*, vol. 43, n° 1, p. 26, 1931.

47 Oyetayo, A. M., Seyifunmi, E. O., Omotayo, F. J., and Olaitan, S. K. 2023. “Effects of Automobile Battery Wastes Disposal on Soil Health Indices”. Advances in Research 24 (6):60-67. https://doi.org/10.9734/air/2023/v24i6985.

48 Radicella SM, Leitinger R. The evolution of the DGR approach to model electron density profiles. Advances in Space Research. 2001 Jan 1;27(1):35-40.

49 Rideout W, Coster A. Automated GPS processing for global total electron content data. GPS solutions. 2006 Jul;10:219-28.